Distributed fiber-optic sensing transforms an abandoned well into a permanent geophysical monitoring array: A case study from Australian South West

Evgenii Sidenko[1], Konstantin Tertyshnikov[1], Boris Gurevich[1], Roman Isaenkov[1], Ludovic P. Ricard[2], Sandeep Sharma[3], Dominique Van Gent[4], and Roman Pevzner[1]

https://doi.org/10.1190/tle41020140.1

Abstract

Distributed temperature sensing (DTS) and distributed acoustic sensing (DAS) data recorded by a fiber-optic array installed during the decommissioning operations of the 1550 m Harvey 3 well in Western Australia reveal an abundance of valuable information about the course of the decommissioning process and the quality of the cement job. The DAS monitoring has detected vibrational disturbances during the cement's setting up, while DTS was used to assess setting up of the cement and curing times as well as uniformity of cementation from the distribution of temperature along the borehole. A weeklong trial acquisition of passive seismic data with the same array a year later shows an abundance of seismic events in a wide frequency range from below 1 mHz to above 200 Hz. The downhole DAS array provides traveltimes and amplitudes of these events, which include earthquakes, mine blasts, ocean microseisms, and local human activity. The amplitudes of waves from distant seismic events can be used to estimate and monitor physical properties of the media along the extent of the well. When used in combination with information from active vertical seismic profiling, these events can help obtain independent estimates of velocities and densities. Spectral analysis of low-frequency microseisms shows a strong correlation between passively recorded DAS and local weather observations. This shows that the ability to continuously record oceanic microseisms at low frequencies opens opportunities to employ such arrays for wave climate studies. In addition, the data contain peculiar in-hole reverberations likely caused by crossflow of groundwater behind the intermediate casing, which may indicate imperfections of the cement job. The results demonstrate that a downhole fiber-optic array installed in an abandoned well represents an opportunity to establish a permanent facility for continuous recording of passive and active geophysical data and for exploring various applications.

Introduction

New wells give an opportunity to gather new information about the subsurface through wireline logging, coring, and borehole geophysical studies. Wells also provide room for installing dedicated sensors to monitor subsurface changes such as those related to oil production or CO_2 geosequestration. Abandonment of previously drilled wells is a costly operation and involves plugging with cement and removal of all infrastructure. As a result, the well, an expensive and formerly precious asset, is lost. However, installation of distributed fiber-optic sensors during decommissioning has potential to transform an abandoned well into a permanent sensor array. This deployment can be used to control the cementation process and monitor subsequent changes in the subsurface by recording such parameters as strain, temperature, and vibration caused by natural or induced seismicity. Such wells also can be utilized to conduct active borehole seismic surveys such as vertical seismic profiling (VSP).

The use of fiber-optic cables as downhole sensors has substantial advantages over conventional downhole receivers. Most fiber-optic cables are robust and reliable for long-term installations as they have no electronics or moving parts. Also, deployment of such cables in a well distributes sensors over its entire length at small spacing intervals. Fiber-optic cables can also be manufactured to withstand considerable pressure and temperature (up to 250°C). The most sensitive and valuable instrument equipment — an optical interrogator unit — is always located at the surface and can be connected easily to the downhole cable and reconfigured to satisfy the measurement requirements. Such benefits make this technology a perfect option for plug and abandon (P&A) monitoring applications and building permanent surveillance arrays in harsh environments such as deep wells. Once deployed, fiber-optic sensing systems can be used for distributed acoustic sensing (DAS) and distributed temperature sensing (DTS).

DTS measures temperature distribution along the fiber-optic cable. Borehole temperature monitoring helps with wellbore and reservoir characterization. Continuous DTS recording can characterize downhole flow operations (Patterson et al., 2017; Miller et al., 2018). DTS can also be used to monitor the cement curing process, which provides near real-time information about the cement injection process, and verify the quality of the cement binding a posteriori (Ricard, 2020).

DAS is designed to measure dynamic strain and uses a single optical fiber as an array of optical vibrational sensors with a dense receiver spacing that could be as small as 0.25 cm (Silixa, 2018). It is capable of acquiring data in a broad frequency range

[1]Centre for Exploration Geophysics, Curtin University, Perth, Western Australia. E-mail: evgenysidenko@gmail.com; konstantin.tertyshnikov@curtin.edu.au; b.gurevich@curtin.edu.au; roman.isaenkov@postgrad.curtin.edu.au; r.pevzner@curtin.edu.au.
[2]CSIRO Energy, Perth, Western Australia. E-mail: ludovic.ricard@csiro.au.
[3]Carbon Projects Pty. Ltd., Perth, Western Australia. E-mail: sandeep_sharma1@outlook.com.
[4]Department of Mines, Industry Regulation and Safety, Perth, Western Australia. E-mail: dvangent54@gmail.com.

from below 1 mHz to hundreds of hertz (Becker et al., 2017; Lindsey et al., 2019). DAS can be used to monitor local and regional seismicity and detect distant seismic events (Ajo-Franklin et al., 2019), record ambient seismic noise, and monitor any borehole-related vibrational signals (Miller et al., 2018; Karrenbach et al., 2019).

Most installations of fiber optics are in open and active monitoring and production wells. Here, we use fiber-optic sensing for monitoring of P&A operations of a deep well and its subsequent transformation into a permanent seismic monitoring array. The study was done during and after decommissioning of the Harvey 3 well drilled as a part of the South West Hub CO_2 geosequestration project in Western Australia (Sharma et al., 2017).

The proposed initiative to cement a fiber-optic cable inside the Harvey 3 well as a part of the decommissioning procedure was supported by the Department of Mines, Industry Regulation and Safety of Western Australia, and the installation was conducted in January 2019. The Harvey 3 well site is located about 120 km south of the state capital of Perth and about 10 km from the coast. Such close proximity to a major city yet away from industrial and traffic noise makes the site an optimal location for establishing a permanent facility for passive seismic data acquisition. During P&A operations, a comprehensive data set was acquired using DAS and DTS to monitor cement flow and curing (Ricard et al., 2019).

One year after completing decommissioning operations, the Harvey 3 fiber-optic cable was used for a weeklong acquisition of passive seismic data (Pevzner et al., 2020b). Although one week is a relatively short time to record a representative data set for analysis of noise patterns and seismicity in the area, many valuable observations and revelations were obtained. In particular, the results demonstrate that ambient seismic signals can reveal information about the well's conditions a year after cementation, distribution of elastic properties along the well, and natural processes such as seismicity and ocean wave climate.

Preliminary results describing installation of the fiber-optic cable DAS and DTS monitoring of P&A operations and one-week passive monitoring conducted a year after the borehole cementation were published in Ricard et al. (2019) and Pevzner et al. (2020b). In this paper, we present a more systematic and complete analysis of the experiment and data.

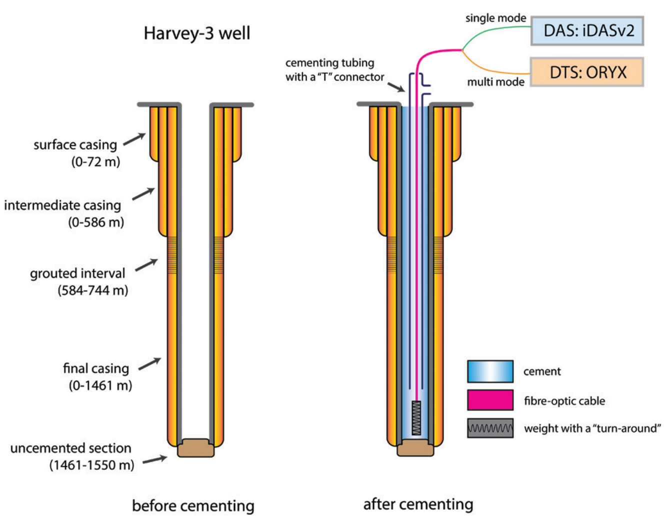

Figure 1. Scheme of Harvey 3 well before and after cementing.

South West Hub project background

The South West Hub Carbon Capture and Storage (CCS) project was the first initiative in Western Australia supported by the Australian Government's CCS Flagships program (Sharma and Van Gent, 2018). The site is located approximately 120 km south of Perth. Several wells were drilled (Harvey 1, 2, 3, and 4) in the project area as part of an extensive program of geologic characterization and uncertainty reduction. The Harvey 1 well was plugged and abandoned in 2011. Harvey 2 is a site of a long-term CSIRO In-Situ Laboratory research facility (Michael et al., 2019). Harvey 3 and Harvey 4 were decommissioned in 2019. Harvey 3 was drilled between December 2014 and June 2015 as a stratigraphic well for geologic characterization of the South West Hub project area. The well reached the top of the target formation for planned CO_2 injections. The well is completed with three stages of casing (Figure 1) including a 4.5 in. production casing. The total depth of the well is 1550 m. The well was left suspended shortly after drilling with van Ruth plugs at the bottom (Nims and Pollock, 2015). The Harvey 3 well and its vicinity area are characterized by a comprehensive suite of data comprising core samples analysis (Singh, 2018), wireline logs, and seismic surveys, including 3D VSP and a dedicated high-resolution 3D surface seismic survey (Urosevic et al., 2017). Availability of such a detailed knowledge base about the site makes it attractive for innovative experiments and trials. Planned decommissioning of the well presented an excellent opportunity to conduct the first trial of transforming an abandoned well into a deep vertical permanent seismic array using fiber-optic sensing technology. The deployed fiber-optic cable acts as a receiver array providing in-situ measurements of the subsurface at thousands of points along the well during and after the P&A process.

Monitoring of the decommissioning process using optical fibers

The fiber-optic cable was installed as a part of Harvey 3 well decommissioning operations on 22 and 23 January 2019. A quarter-inch stainless steel jacketed fiber-optic loose-tube cable has four single-mode and two multimode fiber-optic cores as well as two copper cores.

The fiber-optic cable was terminated with a double-ended configuration for the multimode cores (for DTS measurements) and with attenuators for the single-mode cores (for DAS measurements), while the electrical conductors were connected together to enable heating of the cable (for active DTS measurements). The downhole terminations were inserted inside a 6 m long steel weight for protection and to ease the cable deployment.

Before cementing started, a cementing tubing (2 ⅜ in) was installed to enable the fiber-optic cable deployment inside it. Once the tubing was installed and the fluid swapped, the fiber-optic cable was lowered inside the tubing. A custom-designed T-shaped connection at the wellhead enabled the simultaneous cementing process and its monitoring using distributed fiber-optic sensors.

The tubing was left in the well after the cement injection. A schematic diagram of the Harvey 3 well before and after the cementation is shown in Figure 1.

The primary idea of the experiment was to monitor the borehole P&A (cementing) process using fiber-optic sensing technology.

DTS monitoring. Borehole temperature was monitored for two days including baseline (after cable installation and prior to the cement injection), cement injection, and postinjection (cement curing) using a Sensornet Oryx DTS interrogator with a vertical spacing of 1 m and temporal sampling of 60 s.

Figure 2 shows the DTS data recorded over the P&A operations in the well. Figure 2a shows absolute temperature values measured by DTS; Figure 2b shows the temperature anomaly — absolute temperature minus baseline average (depth temperature distribution). The baseline average was calculated for each depth along the fiber-optic cable and over the time interval before the start of the cement injection (to the left from the first black dashed line in Figure 2). On both plots, the vertical axis corresponds to the length along the fiber-optic cable (measured depth); the horizontal axis corresponds to time. The time interval between the two dashed lines corresponds to the period of the acquired DAS data shown in Figure 3 in the next section. Three different stages can be observed on DTS data plots: (1) baseline, (2) injection and cement settling, and (3) cement curing and equilibration.

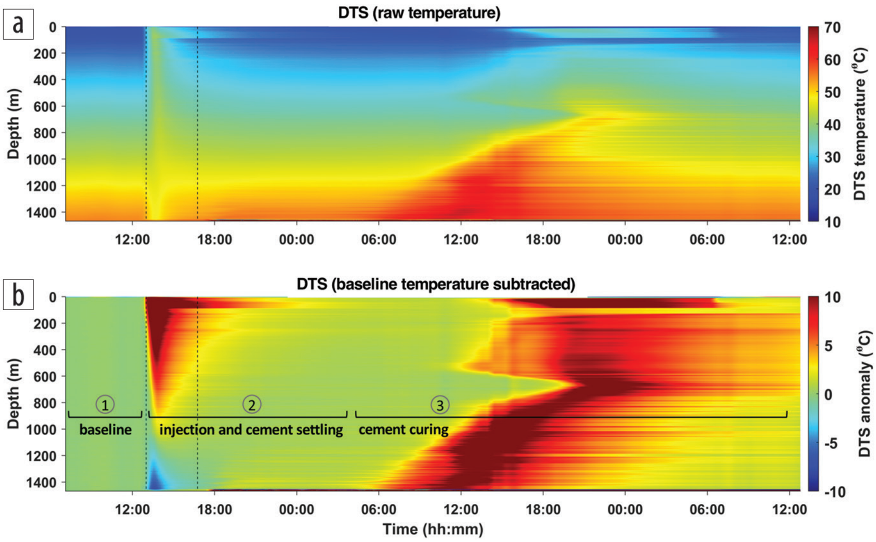

Figure 2. DTS data recorded in Harvey 3 well. (a) Absolute temperature. (b) Temperature change regarding the baseline's average. Dashed interval indicates recorded DAS data time frame.

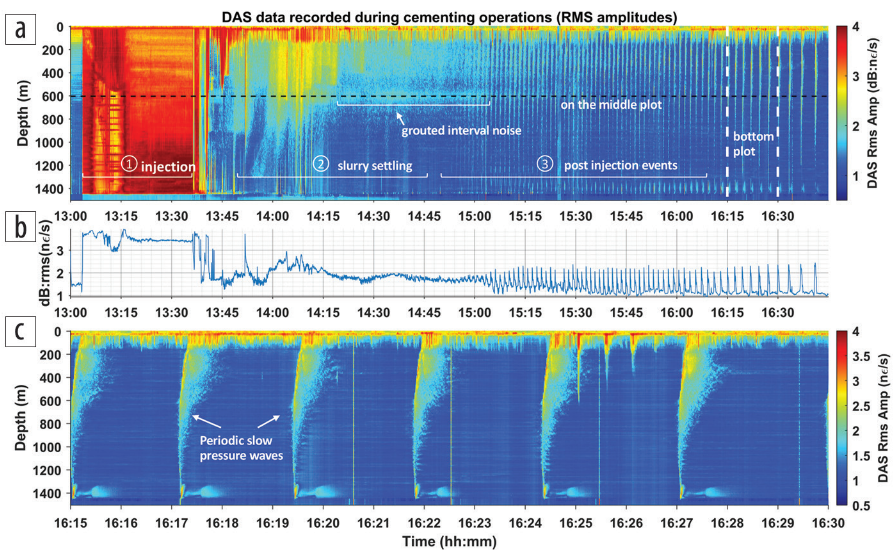

Figure 3. DAS data recorded during Harvey 3 well cementation. (a) DAS root-mean-square amplitudes for the whole well interval starting from the start of the injection; (b) DAS response from a single depth of 600 m (a single trace shown as black dashed line on the upper plot); (c) DAS response from the time interval highlighted by white dashed lines in the upper plot.

Cement temperature was constant over the time of the injection and while it filled the whole well column. From Figure 2 it is clear that the temperature of the cement slurry was equal to the formation temperature at about 1100 m depth (approximately 40°C–45°C). The interval between two dashed lines on the anomaly plot (Figure 2b) shows that the introduction of the cement slurry heated the depth interval above 1100 m and cooled the interval below 1100 m.

After the cement was fully injected, it gradually settled down, and in 12 hours the temperature reversed back to the formation (baseline) values over the entire well length. It took noticeably more time for temperatures in the upper part (0–100 m) to equilibrate, probably because of lower thermal conductivity of the well in this interval due to the presence of the surface casing.

Cement curing started only 18 hours after injection (6:00 to the end of the recording). First, it starts at the bottom of the well, as the formation temperature is the catalyst and it is the highest in the deepest part. Then, the cement curing process starts slowly at each depth all the way up to the wellhead. As cement curing is an exothermic reaction, the DTS data show a clear heat release.

Recorded DTS data help identify two heterogeneities in the well structure. The first occurs between 600 and 800 m as a delay to the start of the curing process in this interval. This depth interval corresponds to the grouted section of the Harvey 3 well (see Figure 1). The second heterogeneity is in the depth interval around 100 m. This section corresponds to a joint between intermediate and surface casings. DTS data acquired in this interval show very little temperature change compared to other parts of the well.

Overall, fiber-optic temperature monitoring data acquired during P&A operations demonstrate that this method is a simple and reliable tool to monitor the process of cement curing along the entire borehole. Real-time DTS data help diagnose cement conditions and better assess the actual cementation time. This is important to ensure that the pipe is not moved before the cement is fully set and reduces the chances of developing of channels allowing flow in cement behind casing.

DAS monitoring. DAS monitoring of the decommissioning process used single-mode fibers and two different interrogators: Fotech Helios Theta and Silixa iDAS v2. Monitoring acquisition started at 10:00 on 23 January and completed by 17:00 on the same day. The recorded DAS data are shown in Figure 3. The time-lapse response from the interrogators over a nearly 4-hour time interval is shown in Figure 3a.

Surface activities near the wellhead are indicated by short red bursts at the 0–200 m depth interval. Cement injection lasted for 30 minutes from 13:05 until 13:35. The injection process is clearly visible on DAS as a red intensive area along the entire length of the well. The response to the injection is uniform along the entire length of the borehole and is hard to interpret as it is primarily related to vibrations of the cementing tubing.

After the cement has been injected, various responses at different parts of the well can be observed (13:45–14:45). In this time interval, the DAS response is not uniform along the borehole and probably is related to the cement slurry settling down in the well. We can observe short-period oscillations in the lower part of the well (below 1000 m) and more long-period signals in the upper part (0–800 m).

To improve borehole integrity, during the well drilling in 2015, the depth interval from 584–744 m was relatively soft and friable and thus was grouted with the cement and redrilled (Nims and Pollock, 2015). We can see the presence of some distinct noise related to this interval around 600 m depth between 14:30 and 15:15.

The final time interval of DAS monitoring between approximately 15:00 and 16:45 shows a completely different behavior compared to the previous parts of the record. During this time, DAS recorded a number of slow periodical events propagating along the fiber-optic cable. The time gap between these events is gradually increasing toward the end of the DAS record from approximately 1–2 to 3–4 minutes. Several events recorded during this time interval, indicated by two white dashed lines in Figure 3a, are shown in Figure 3c. The apparent propagation velocity of these events along the cable up to the wellhead is less than 100 m/s. This is much lower than for any typical body or surface seismic waves. These events are most possibly slow pressure waves occurring in the water-gas mixtures (Boone et al., 2014). The velocity of pressure waves in water-gas mixtures depends on temperature, pressure, and gas void fraction. The presence of air bubbles dramatically decreases the pressure-wave velocity, which can be as low as 20 m/s (Kieffer, 1977).

The character of the observed periodic events was changing with time as shown in Figure 4. At the beginning (Figure 4a), it is mostly shapeless scattered noise with no distinct front. After approximately 15:04, a front gradually appears (first-break arrivals of the events) along the entire length of the well (Figure 4b). After 16:00, the front becomes clear: most of the energy is concentrated around first-break arrivals (Figure 4c). Scattered noise becomes denser in the upper part, and it becomes evident that this noise is related to these periodic events. Traveltime curves are not symmetric along the borehole length. Their zero time corresponds to the depth interval between 800 and 1200 m. The apparent velocity is lower in the upper part of the well as manifested by a more noticeable curvature of first-break arrivals. Such a time evolution of the described events could be caused by varying borehole conditions (pressure, temperature, gas bubbles' fraction). Also, different noise patterns can be observed in the upper half of the cable and in the vicinity of the bottom hole. The noise is much more scattered after first-break arrivals in the upper part of the well. There are second-order events occurring near the bottom hole. These deeper events could occur because of the interaction between the cable and the bottom hole. Temperature variations also causes a signal on DAS (shown in Figure 4b). Such short-period events cannot be validated by DTS as it has a much larger sampling rate (60 s).

The acquired DAS data are quite rich in events but also quite complex and require further studies to gain more understanding and develop an appropriate approach for analysis. Nevertheless, even this qualitative examination provides new insights into the interaction between a fiber-optic cable and injected cement slurry and even into the mechanical behavior of the whole cemented borehole system. It is also important that DAS data are usually acquired with much denser temporal sampling than DTS (1 ms versus 30 s). Thus, DAS can easily track not only seismic vibrations but also signals caused by short-period temperature changes, as DAS is sensitive to the time derivative of the temperature (Miller et al., 2018; Sidenko et al., 2021).

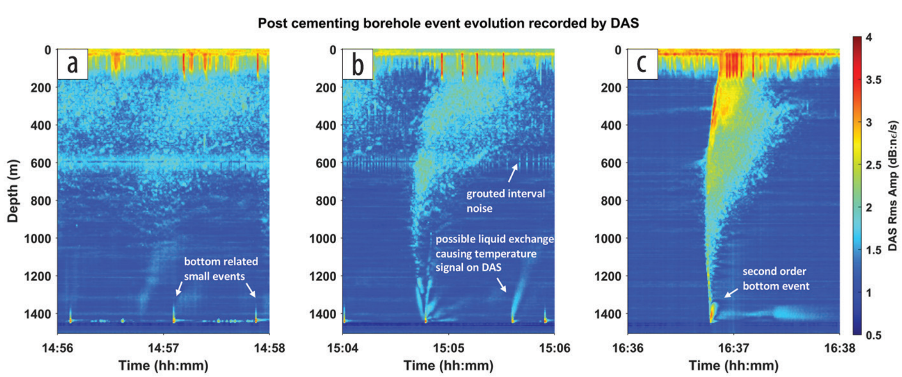

Figure 4. Evolution of the borehole event recorded by DAS after cementing operations were finished.

Passive data acquisition

In May 2020, more than one year after the completion of the P&A operations, passive DAS acquisition was conducted using the fiber-optic array cemented in the Harvey 3 well. The main objective of the experiment was to further explore the feasibility and potential of passive borehole seismic monitoring using the cable in the abandoned borehole.

The passive DAS survey was acquired using only the Silixa iDAS v2 interrogator. The DAS recording unit was housed in a seismic acquisition truck and powered from a diesel generator on a trailer positioned away from the truck to reduce vibration on the interrogators. The equipment was controlled remotely using a cellular network.

Data acquisition commenced on 21 May and finished on 28 May. No data were acquired for one day around 24 May due to a once-in-a-decade storm (Manfield et al., 2020) passing through the area, which forced suspension of the operation.

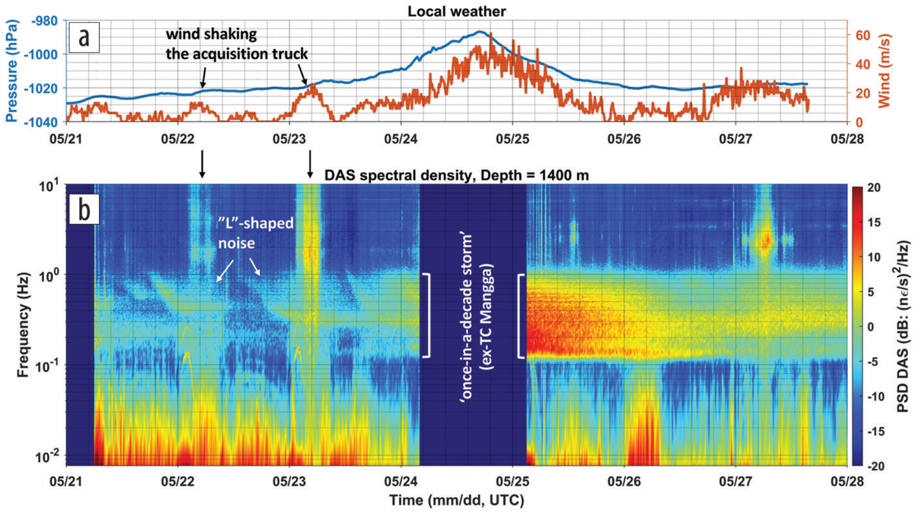

Figure 5. (b) Spectrogram of the DAS record at 1400 m MD compared to (a) weather events.

Passive seismic data analysis consists of identification of site-specific components of the wavefield, which can be used to derive useful information about the subsurface, conditions of the well, or human-related and natural events. As a result, three major groups of events were identified in the recorded data set: (1) ocean-related low-frequency microseisms, (2) distant mine blasting and earthquakes, and (3) local surface human-related activity and in-well repeating events.

Oceanic microseisms. Figure 5 shows a spectrogram of DAS data (Figure 5b) computed for the receiver at 1400 m along with information about the weather in the area (Figure 5a). The frequency range between 0.1 and 1 Hz is dominated by Rayleigh waves corresponding to the oceanic microseisms (Bromirski, 2002; Nishida, 2017; Glubokovskikh et al., 2021) represented by the double frequency of the actual ocean waves spectrum (Lin et al., 2018). They originate from the coastal surface oscillations generated by nonlinear interference between oppositely propagating ocean waves of the same frequency (Hasselmann, 1963). The spectrogram also demonstrates the ability of fiber-optic sensors to record very low frequencies (down to 10 mHz), which can carry useful information about the oceanic climate.

The spectrogram contains clearly pronounced L-shaped spectral associated with a sea breeze on 22 and 23 May as well as clear evidence of a big storm on 24 and 25 May. The increased wideband noise at approximately 2–3 Hz is related to the resonance of the acquisition truck forced by the strong wind with speeds above approximately 25 km/h.

Arrivals of remote storms are characterized by the spectral peak shifting toward the higher frequencies due to the deepwater ocean waves' dispersion and distinguished by L-shaped patterns (Bromirski et al., 1999) of the oceanic noise recorded between 21 and 24 May. In contrast, the development of a large local storm is indicated by the spectral peak shift toward the lower frequencies. It is accompanied by the dramatic increase of wind speed (Figure 5a) as the intensity of the local storm increases.

Mine blasting and earthquakes. Eight blasting events from mines located 40–70 km from the site were detected on

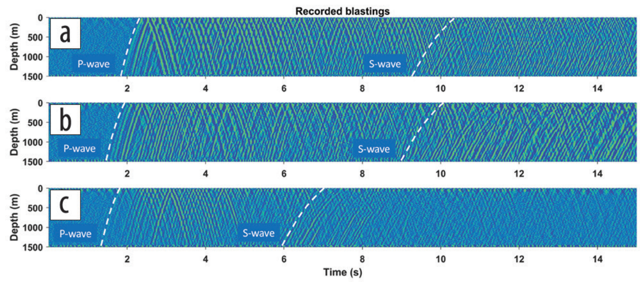

Figure 6. Examples of blasting events recorded by the permanently installed fiber-optic array.

seismograms using a semblance-based algorithm. Three examples of such events are shown in Figure 6. Both P- and S-waves are clearly pronounced on the record and can be identified by the difference in the apparent velocities. The delay between P- and S-wave arrival times allows estimating the distance to the source. To do this, we use a velocity model that was previously calibrated using several regional earthquakes recorded by a training well at the Curtin campus approximately 120 km away from Harvey 3 (Shulakova et al., 2020).

DAS also recorded several earthquakes. To identify earthquakes in data, we matched the times of the events to Geoscience Australia's Earthquake Database (Geoscience Australia, 2020). Figure 7 shows an example of a distant earthquake (the Banda Sea earthquake with magnitude Mw = 5.42). Figure 7 shows the earthquake signal recorded by DAS at 500 m depth; Figure 7b shows the corresponding DAS response spectrogram; Figure 7c shows the signal recorded at the same time by the vertical component of the broadband high-gain seismometer located 10 km from the well in the town of Harvey (Balfour et al., 2014). Both DAS and seismometer data are band-pass filtered to emphasize body waves arrivals. In DAS data, the P-wave first arrival looks more distinct than in the seismometer data as DAS receivers are located in a quiet downhole environment away from surface wave noise.

Recorded waves from distant blasting events and natural earthquakes can be used to monitor variations of elastic properties along the well over time (Mateeva and Zwartjes, 2017; Pevzner et al., 2020a). The DAS amplitude is inversely proportional to the acoustic quantity

$$(A_{DAS})^{-1} \sim (\rho V_P^3)^{0.5}, \tag{1}$$

where ρ is the density and V_P is the compressional wave velocity. The downhole DAS array records these regularly occurring events (particularly blasting, which has a firm daily schedule) with a very high signal-to-noise ratio and provides a clear path for practical monitoring of the near-well formation properties.

A comparison of elastic properties from wireline log data and DAS amplitude for one of the blasting events is shown in Figure 8. Note that the lower amplitude (higher inverse amplitude) in the section above 586 m corresponds to the intermediate casing and may indicate poorer coupling between borehole and the formation in this section. Each event may have different absolute amplitude and the measurement provides only a relative spatial variation.

Repeating surface events. Several surface seismic events associated with human activity were detected during the trial. Figure 9 shows examples of those events.

Figures 9a and 9b show P- and S-waves whereas Figure 9c has only the S-wave. The shape of the P-waves traveltime curves suggests that these events originated at the surface not too far from the well. Figure 10a shows a stack of eight repeated events found within the recorded data set compared to a single shot (with similar offset) from 3D VSP data acquired in 2017 from the same well using a 26,000 lb vibroseis source and conventional geophones (Figure 10b).

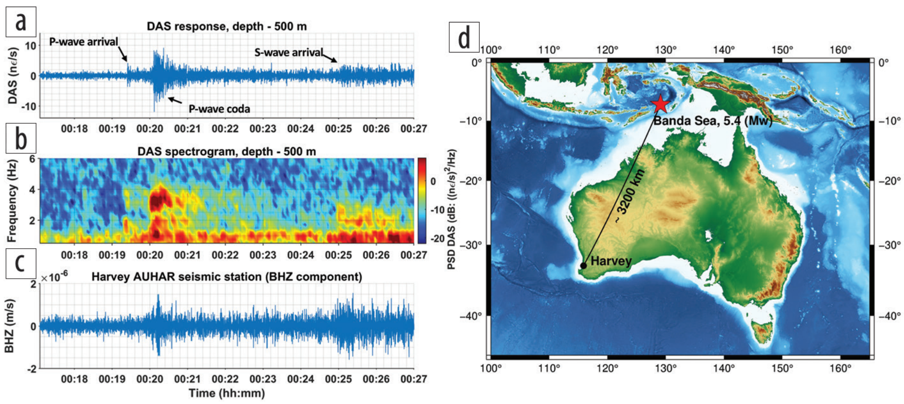

Figure 7. Example of the teleseismic event recorded by fiber optics in the abandoned Harvey 3 well. (d) Earthquake epicenter location relatively to Harvey, WA. (a) Time-series response of a single DAS channel at 500 m depth. (b) Spectrogram of the DAS trace. (c) Vertical component recorded by the local seismic station located in St Anne's School, Harvey, WA.

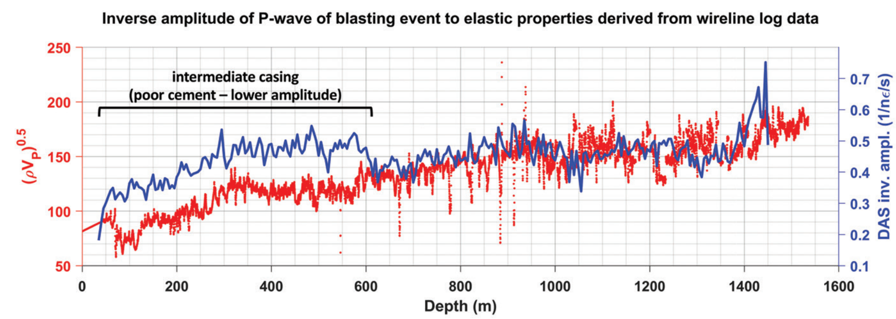

Figure 8. Inverse amplitude of P-wave produced by blasting event on 24 May compared to elastic properties (ρV_P^3)0.5 derived from wireline log data.

Having small-offset surface events recorded by DAS gives an opportunity to derive a velocity profile of the P- and, potentially, S-waves. Figure 11 shows the comparison between P-wave velocity profiles from the sonic log data and estimated from the passive DAS recordings. Joined analysis of the traveltimes from the near-offset events and amplitudes from distant blasts and earthquakes has a potential to provide independent estimates of both velocities and densities of near-well formations and their variation over time. Quality of the passive VSP data can be improved by stacking more repeating events potentially reaching the point that we can also use reflected waves for imaging purposes.

In-well repeating impulse events. DAS also recorded some unexpected events (Figure 12). Their central frequency is close to 200 Hz, while the symmetrical straight-line traveltime curve indicates that the source is located in the wellbore itself (or very close to

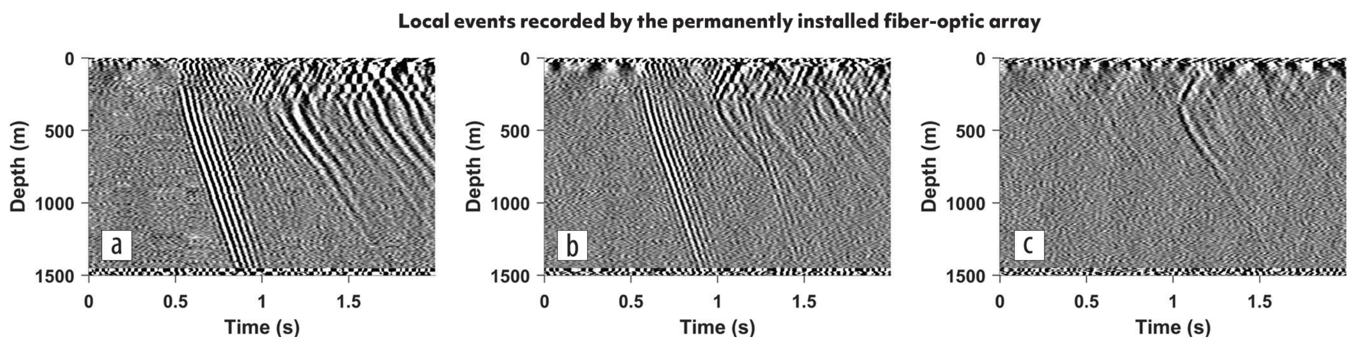

Figure 9. Local events recorded in Harvey 3 well.

it). The depth of the sources varies from 200 to 385 m, and the energy propagates up and down the wellbore within the depth interval corresponding to the intermediate casing. The apparent velocity of the propagating wave is 4.5 km/s, which is typical for a tube wave traveling within the casing.

Overall, 14 such events were detected. The existence of the events may indicate some defects in the quality of the cement between the main and intermediate casing strings. Similar events were described by Bakulin and Korneev (2008) in which unwanted cracks and channels lead to fluid exchange through developing conduits in the cement behind the casing (known as "crossflow"). The crossflow is caused by the pressure difference between different formations. This is an important observation for monitoring P&A wells and can be used immediately in similar situations.

Discussion and conclusions

Installation of a fiber-optic cable in the Harvey 3 well provided a unique opportunity to monitor P&A operations, verify the quality of the cement job, and create a permanent seismic and temperature sensor for future passive and active geophysical surveys.

Fiber-optic-sensing data recorded during the cementing operations reveal an abundance of valuable information about the course of the decommissioning process and the quality of the cement job. The DAS monitoring has detected vibrational disturbances during the cement's setting up, while DTS helped to assess setting up of the cement and curing times as well as uniformity of the cementation. However, DTS has relatively coarse temporal sampling; using finer sampling in DTS might be useful to help identify the origin of some anomalies recorded at the same time by DAS.

A subsequent weeklong trial acquisition of passive seismic data using the previously installed vertical sensing array shows an abundance of seismic events in a wide frequency range including the ultra-low part of the spectrum down to at least approximately 10 mHz. The downhole DAS array allows an analysis of the depth variation of traveltimes and amplitudes of these events, which include earthquakes, mine blasts, ocean microseisms, and local human activity.

The amplitudes of waves from distant seismic events can be used to estimate and monitor physical properties of the media along the entire extent of the well. When used in combination with active

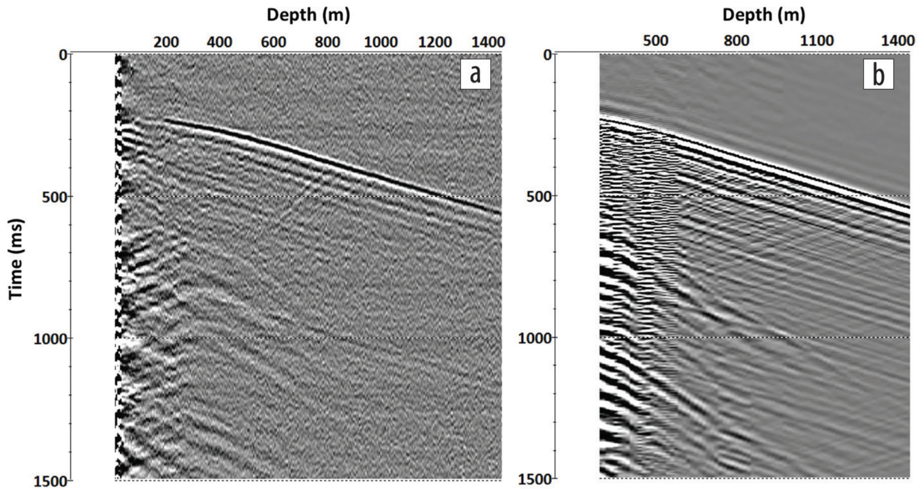

Figure 10. (a) Stack of eight repeating surface events recorded by the cemented fiber-optic array compared to (b) active VSP data acquired in 2017 from the same offset using 26,000 lb vibroseis and 3C geophones.

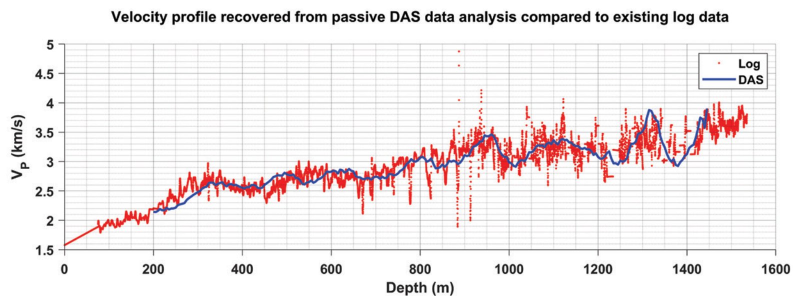

Figure 11. Velocity profile recovered from passive DAS data analysis (blue) compared to existing log data (red).

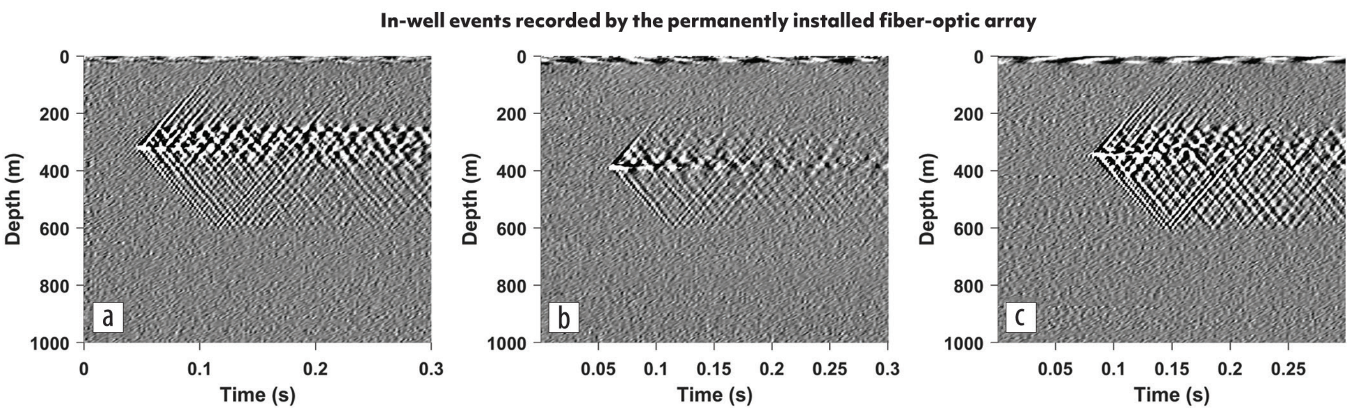

Figure 12. High-frequency in-well events propagating within the intermediate casing section and recorded by the fiber-optic array.

VSP acquired using either controlled or a random source of energy located near the well, these events can help obtain independent estimates of velocities and densities.

Spectral analysis of low-frequency microseisms shows a strong correlation between passively recorded DAS and local weather observations. This shows that the ability to continuously record oceanic microseisms at low frequencies opens up opportunities to employ such arrays for wave climate studies.

In addition, the data contain peculiar in-hole reverberations likely caused by crossflow of groundwater behind the intermediate casing, which may indicate imperfections of the cement job. This information can be used to better understand fluid flows and identify any early onsets of corrosion or other damage, which may be useful as preventive measure in producing wells. Such information can also be considered in a future well design.

The Harvey 3 site is located not far from a population center in an extensively studied area away from urban noise. Thus, the downhole fiber-optic array represents an opportunity to establish an excellent diagnostic facility for continuous recording of passive and active geophysical data and for exploring various applications. For example, a group of wells instrumented with fiber-optic sensors can be utilized for multilateration of regional earthquakes and mine blasts.

Overall, the variety of observations made during this study indicates a strong potential of such installations for many applications. At the moment of writing, we are not aware of another public-domain example with integrated, postabandonment analysis using distributed fiber-optic sensing technology. The bigger picture is that any onshore well coming for P&A can be equipped with a fiber-optic cable. This can provide an opportunity to build a continent-scale network of vertical sensing arrays gathering information about seismic events, global heat flow, and crustal state of stress. TLE

Acknowledgments

The authors are grateful to the Department of Mines, Industry Regulation and Safety of Western Australia for partially funding the work. Parts of this research also have been supported by Curtin Reservoir Geophysical Consortium and the Mineral Exploration Cooperative Research Centre whose activities are funded by the Australian Government's Cooperative Research Centre Program. Seismic data were retrieved from the AusPass archive (http://auspass.edu.au/) under a Creative Commons Attribution 4.0 International license (CC BY 4.0: https://creativecommons.org/licenses/by/4.0/). The data from the AuSIS network were discussed in the "Mine blastings and earthquakes" section. E. S. thanks Curtin Oil and Gas Innovation Centre for providing a PhD scholarship. We are also grateful to Silixa Ltd. for providing iDAS interrogator for our studies.

Data and materials availability

Some data associated with this research are available and can be obtained by contacting the corresponding author.

Corresponding author: evgenysidenko@gmail.com

References

Ajo-Franklin, J. B., S. Dou, N. J. Lindsey, I. Monga, C. Tracy, M. Robertson, V. Rodriguez Tribaldos, et al., 2019, Distributed acoustic sensing using dark fiber for near-surface characterization and broadband seismic event detection: Scientific Reports, **9**, 1328, https://doi.org/10.1038/s41598-018-36675-8.

Bakulin, A., and V. Korneev, 2008, Acoustic signatures of crossflow behind casing in commingled reservoirs: A case study from Teapot Dome: Geophysics, **73**, no. 4, E145–E152, https://doi.org/10.1190/1.2940154.

Balfour, N. J., M. Salmon, and M. Sambridge, 2014, The Australian seismometers in schools network: Education, outreach, research, and monitoring: Seismological Research Letters, **85**, no. 5, 1063–1068, https://doi.org/10.1785/0220140025.

Becker, M., T. Coleman, C. Ciervo, M. Cole, and M. Mondanos, 2017, Fluid pressure sensing with fiber-optic distributed acoustic sensing: The Leading Edge, **36**, no. 12, 1018–1023, https://doi.org/10.1190/tle36121018.1.

Boone, K., A. Ridge, R. Crickmore, and D. Onen, 2014, Detecting leaks in abandoned gas wells with fibre-optic distributed acoustic sensing: International Petroleum Technology Conference, IPTC-17530-MS, https://doi.org/10.2523/IPTC-17530-MS.

Bromirski, P. D., 2002, The near-coastal microseism spectrum: Spatial and temporal wave climate relationships: Journal of Geophysical Research, **107**, no. B8, ESE 5-1–ESE 5-20, https://doi.org/10.1029/2001JB000265.

Bromirski, P. D., R. E. Flick, and N. Graham, 1999, Ocean wave height determined from inland seismometer data: Implications for investigating wave climate changes in the NE Pacific: Journal of Geophysical Research: Oceans, **104**, no. C9, 20753–20766, https://doi.org/10.1029/1999JC900156.

Geoscience Australia, 2020, Earthquakes@GA, https://earthquakes.ga.gov.au, accessed 3 February 2021.

Glubokovskikh, S., R. Pevzner, E. Sidenko, K. Tertyshnikov, B. Gurevich, S. Shatalin, A. Slunyaev, and E. Pelinovsky, 2021, Downhole distributed acoustic sensing provides insights into the structure of short-period ocean-generated seismic wavefield: Journal of Geophysical Research: Solid Earth, **126**, no. 12, e2020JB021463, https://doi.org/10.1029/2020JB021463.

Hasselmann, K., 1963, A statistical analysis of the generation of microseisms: Reviews of Geophysics, **1**, no. 2, 177–210, https://doi.org/10.1029/RG001i002p00177.

Karrenbach, M., S. Cole, A. Ridge, K. Boone, D. Kahn, J. Rich, K. Silver, and D. Langton, 2019, Fiber-optic distributed acoustic sensing of microseismicity, strain and temperature during hydraulic fracturing: Geophysics, **84**, no. 1, D11–D23, https://doi.org/10.1190/geo2017-0396.1.

Kieffer, S. W., 1977, Sound speed in liquid-gas mixtures: Water-air and water-steam: Journal of Geophysical Research, **82**, no. 20, 2895–2904, https://doi.org/10.1029/JB082i020p02895.

Lin, J., S. Fang, X. Li, R. Wu, and H. Zheng, 2018, Seismological observations of ocean swells induced by typhoon Megi using dispersive microseisms recorded in coastal areas: Remote Sensing, **10**, no. 9, 1437, https://doi.org/10.3390/rs10091437.

Lindsey, N. J., T. C. Dawe, and J. B. Ajo-Franklin, 2019, Illuminating seafloor faults and ocean dynamics with dark fiber distributed acoustic sensing: Science, **366**, no. 6469, 1103–1107, https://doi.org/10.1126/science.aay5881.

Manfield, E., G. De Poloni, and J. Hayes, 2020, Ex-Tropical Cyclone Mangga set to bring "once-in-a-decade" storm to Western Australia, https://www.abc.net.au/news/2020-05-23/ex-tropical-cyclone-mangga-brings-one-in-a-decade-storm-to-wa/12279544, accessed 22 December 2021.

Mateeva, A., and P. M. Zwartjes, 2017, Depth calibration of DAS VSP channels: A new data-driven method: 79th Conference and

Exhibition, EAGE, Extended Abstracts, https://doi.org/10.3997/2214-4609.201701201.
Michael, K., A. Avijegon, L. Ricard, M. Myers, K. Tertyshnikov, R. Pevzner, J. Strand, et al., 2019 In-Situ Laboratory for CO_2 controlled-release experiments and monitoring in a fault zone in Western Australia: 2nd Australasian Exploration Geoscience Conference, ASEG Extended Abstracts, https://doi.org/10.1080/22020586.2019.12073207.
Miller, D., T. Coleman, X. Zeng, J. Patterson, E. Reinisch, H. Wang, D. Fratta, et al., 2018, DAS and DTS at Brady Hot Springs: Observations about coupling and coupled interpretations: 43rd Stanford Workshop on Geothermal Reservoir Engineering Stanford Geothermal Workshop.
Nims, P., and M. Pollock, 2015, Harvey-3 final well report: Department of Mines and Petroleum.
Nishida, K., 2017, Ambient seismic wave field: Proceedings of the Japan Academy, Series B, **93**, 423–448, https://doi.org/10.2183/pjab.93.026.
Patterson, J. R., M. Cardiff, T. Coleman, H. Wang, K. L. Feigl, J. Akerley, and P. Spielman, 2017, Geothermal reservoir characterization using distributed temperature sensing at Brady Geothermal Field, Nevada: The Leading Edge, **36**, no. 12, 1024a1–1024a7, https://doi.org/10.1190/tle36121024a1.1.
Pevzner, R., B. Gurevich, A. Pirogova, K. Tertyshnikov, and S. Glubokovskikh, 2020a, Repeat well logging using earthquake wave amplitudes measured by distributed acoustic sensors: The Leading Edge, **39**, no. 7, 513–517, https://doi.org/10.1190/tle39070513.1.
Pevzner, R., K. T. Tertyshnikov, E. Sidenko, R. Isaenkov, S. Glubokovskikh, L. Ricard, B. Gurevich, S. Sharma, and D. Van Gent, 2020b, Underground sounds from an abandoned well: Forensic analysis of distributed acoustic sensing data: EAGE Workshop on Fiber Optic Sensing for Energy Applications in Asia Pacific, https://doi.org/10.3997/2214-4609.202070026.
Ricard, L. P., 2020, Using distributed temperature sensing to inform the quality of cementing operations: SPE Asia Pacific Oil and Gas Conference and Exhibition, SPE-202350-MS, https://doi.org/10.2118/202350-MS.
Ricard, L., R. Pevzner, E. Sidenko, K. Tertyshnikov, S. Sharma, D. Van Gent, and R. Isaenkov, 2019, Transforming an abandoned well into a permanent downhole receiver array: Harvey-3 case study: ASEG Extended Abstracts, https://doi.org/10.1080/22020586.2019.12073043.
Sharma, S., and D. Van Gent, 2018, The Australian South West Hub Project: Developing confidence in migration assisted trapping in a saline aquifer — Understanding uncertainty boundaries through scenarios that stress the models: 14th International Conference on Greenhouse Gas Control Technologies, GHGT-14, https://doi.org/10.2139/ssrn.3366170.
Sharma, S., D. Van Gent, M. Burke, and L. Stelfox, 2017, The Australian South West Hub Project: Developing a storage project in unconventional geology: Energy Procedia, **114**, 4524–4536.
Shulakova, V., K. Tertyshnikov, R. Pevzner, Y. Kovalyshen, A. Bona, and B. Gurevich, 2020, Ambient seismic noise in urban environment: Case study using downhole DAS at Curtin University campus: EAGE Workshop on Fiber Optic Sensing for Energy Applications in Asia Pacific, https://doi.org/10.3997/2214-4609.202070019.
Sidenko, E., R. Pevzner, K. Tertyshnikov, and M. Lebedev, 2021, Effects of temperature on DAS measurements: Second EAGE Workshop on Distributed Fibre Optic Sensing, https://doi.org/10.3997/2214-4609.202131018.
Silixa, 2018, iDAS datasheet, https://silixa.com/wp-content/uploads/iDAS-datasheet-2018-2.pdf, accessed 22 December 2021.
Singh, A., 2018, Final report, special core analysis, selected samples from Wells DMP Harvey-1, DMP Harvey-3 , and DMP Harvey-4 Western Australia: Prepared for Department of Mines and Petroleum, https://www.dmp.wa.gov.au/documents/community-education/Harvey-1-3-4-SCA-Report-Corelab.pdf, accessed 17 January 2022.
Urosevic, M., S. Ziramov, R. Pevzner, K. Tertyshnikov, D. Popik, and D. Van Gent, 2017, CO_2 storage site characterisation at the location of Harvey-3 well, Harvey, Western Australia: EAGE/SEG Research Workshop 2017, https://doi.org/10.3997/2214-4609.201701945.